Drive by Blind Modal Identification with Singular Spectrum Analysis

Jiantao Li[1], Xinqun Zhu[2], Siu-seong Law[3] and Bijan Samali[4]

[1]PhD student, School of Civil and Environmental Engineering, University of Technology Sydney, Broadway, NSW 2007, Australia. Email: jiantao.li@student.uts.edu.au

[2]Associate Professor, M.ASCE, School of Civil and Environmental Engineering, University of Technology Sydney, Broadway, NSW 2007, Australia. Email: xinqun.zhu@uts.edu.au

[3] Professor, School of Civil Engineering, Chongqing University, China. E-mail: siu-seong.law@connect.polyu.hk

[4] Professor, School of Computing, Engineering & Mathematics, Western Sydney University, Penrith, NSW2751, Australia. E-mail address: b.samali@westernsydney.edu.au

Abstract

The drive-by bridge parameter identification has been an active research area in recent years. An instrumented vehicle passing over a bridge deck captures the dynamic information of the bridge structure without bridge closure and onsite instrumentation. The vehicle dynamic response includes components associated with the bridge surface roughness, and the vehicle and bridge vibration. It is a big challenge to separate these components and extract the bridge modal parameters from the vehicle response. A novel drive by blind modal identification with singular spectrum analysis is proposed to extract the bridge modal frequencies from the vehicle dynamic response. The single-channel measured vehicular response is decomposed into a multi-channel dataset using SSA, and the bridge frequencies are then extracted via the blind modal identification. Numerical results show that the proposed method is effective and robust to extract the bridge frequencies from the vehicle response measurement even with Class B road surface roughness. The effects of the moving speed and the vehicle parameters on the identification are also studied. A vehicle-bridge interaction model in the laboratory is also studied to further verify the proposed method using one and two axle vehicles.

Keywords

Vehicle-bridge interaction, drive by blind modal identification, singular spectrum analysis, road surface roughness, instrumented vehicle.

Introduction

Indirect bridge monitoring, also referred to as “drive by bridge health monitoring” has been an active field of research in recent years (Malekjafarian et al., 2015). Unlike the conventional direct approach, the sensor is installed on the axle of vehicle instead of the bridge deck. This indirect method is cost-effective and convenient compared to the direct approach. There is a big potential for a quick scan of bridges in the road network using the instrumented vehicle. The identification of bridge modal parameters is a critical part for vibration-based structural health monitoring (SHM). Yang et al. (2004) pioneered an indirect approach to extract natural frequencies of bridge structures from the acceleration response of a vehicle during its passage over the bridge deck. The response of the moving vehicle contains dynamic information of the structure. However, when the vehicle moves on a rough bridge deck, the vehicular frequency is usually dominating in its response spectrum and it masks the bridge frequency components. Yang et al. (2012) used the technique of subtracting the responses or the response spectra of two successive vehicles to mitigate the impacts of road surface roughness on the identification of bridge frequencies. However, the elimination or reduction of the road surface roughness effect is still a big challenge which needs further study for practical application of the indirect method, especially with only one instrumented vehicle (Zhu and Law, 2015; Yang and Yang, 2018).

The blind source separation (BSS) has been a promising tool for the output-only modal identification (Sadhu et al., 2017) in last decade. BSS is originally used to recover special source components from the measured data, and the second-order blind identification (SOBI) is used to solve the BSS problem (Antoni, 2005). The mathematical equivalence between the modal expansion theorem and the BSS methods has been studied (Kerschem et al., 2007; Poncelet et al., 2007). The SOBI algorithm could produce components that are mathematic equivalent with structural modal responses from the measured data without any modifications (Zhou and Chelidze, 2007). A framework for output-only blind modal identification (BMID) was developed basing on the SOBI (McNeil and Zimmerman, 2008). Structural modal frequencies and damping ratios were estimated from modal response related components. Recently, BSS has been modified and applied to non-stationary problems (Hazra et al., 2009; Yang and Nagarajaiah, 2012). It needs to have enough independent observations that the number of sensors should be equal or greater than the number of modes (McNeil and Zimmerman, 2008). When considering the drive-by bridge modal parameter identification using one instrumented vehicle, only one sensor is installed on the vehicle and one single channel of measurement is available. To solve the underdetermined problems where the number of observations is less than the number of active components, the sparsity of sources is widely exploited in time-frequency domain (Zhen et al., 2017). Wang and Hao (2013) proposed a structural damage identification method based on compressive sensing (CS). The application of CS relies on the sparsity of signals in a transform domain. In this paper, to extract the independent components for the bridge modal frequency identification with one moving sensor in time domain, a pre-process to construct multi-channel datasets from the single channel measurement is required before applying the BMID method.

The singular spectrum analysis (SSA) is a data analysis technique that can decompose a set of time-series data into a finite number of interpretable components in time-domain ordered by their corresponding singular values (Liu et al., 2014). The obtained components represent the trends, oscillatory components, noises or others. When the vehicle moves over a rough deck surface, the spectrum of the vehicle response contains a dominant component related to the vehicular frequency. This component is taken as the "trend" which masks the bridge-related frequencies in the spectrum (Yang et al., 2013). Yang et al. (2013) used SSA to filter the vehicle response component for improving the visibility of bridge response components. However, under- or over-filtering may happen with the grouping. In this study, the vehicular response is decomposed into a number of components as a multi-channel dataset which will be analysed with the BSS to identify the bridge modal frequencies.

Some researches have been conducted on the effect of some influential factors on the drive-by bridge frequency identification, i.e. road surface roughness, vehicle properties, the moving speed, ongoing traffic, and the measurement noise (Chang et al., 2010; Malekjafarian and Obrien, 2017). To the best knowledge of the authors, there is little research on the component analysis of the measured vehicular response for the bridge modal frequency identification. In this paper, the single channel measurement based blind modal identification method is proposed to extract the bridge modal frequencies from dynamic responses of the vehicle passage over the bridge deck. The SSA technique is used to separate the vehicle response into multiple independent components which are then input into the BSS to extract the modal responses for the indirect identification of the bridge modal frequency. Numerical and experimental studies with a vehicle-bridge interaction model in the laboratory are conducted to verify the proposed method. The effects of some influential system parameters on the identification are also investigated.

Theoretical background

Equation of motion for the bridge

The equation of motion for the bridge is given (Zhu and Law, 2002) as

$$\mathbf{M}_b\ddot{\mathbf{d}}_b + \mathbf{C}_b\dot{\mathbf{d}}_b + \mathbf{K}_b\mathbf{d}_b = \mathbf{F} \tag{1}$$

where $\mathbf{M}_b$, $\mathbf{C}_b$, $\mathbf{K}_b$ are the mass, damping and stiffness matrices of the bridge, respectively; $\boldsymbol{F}$ is the vector of interaction forces acting on the bridge due to the traffic excitation. $\mathbf{d}_b, \dot{\mathbf{d}}_b, \ddot{\mathbf{d}}_b$ are the vectors of displacement, velocity and acceleration responses of the bridge respectively.

The displacement of the bridge can be expressed as follows with the modal superposition method (Clough and Penzien, 1975)

$$d_b(x,t) = \sum_{i=1}^{N} \phi_i(x)\, Y_i(t) \tag{2}$$

where N is the number of vibration modes considered. $\phi_i(x), Y_i(t)$ are the ith mode shape and modal response, respectively.

Substituting Eq. (2) into Eq. (1) and applying the orthogonality conditions, Eq. (1) becomes:

$$\ddot{Y}_i + 2\xi_i\omega_i\dot{Y}_i + \omega_i^2 Y_i = P_i(t) \tag{3}$$

where $\omega_i, \xi_{i,} M_i$ are the ith modal frequency, damping ratio and the modal mass of the bridge. The modal force is given by $P_i(t) = \int_0^L F(x,t)\emptyset_i(x)dx\,/M_i$ and $F(x,t)$ is the traffic excitation.

Equation of motion for the instrumented vehicle

The instrumented vehicle is assumed to move over the deck at a constant speed v, as shown in Figure 1. The vehicle is modelled as a quarter-car model with single-degree-of-freedom (SDOF). The equation of motion for the vehicle can be obtained as:

$$m_v\ddot{d}_v(t) + c_v\dot{d}_v(t) + k_v d_v(t) = \left\{c_v\left[\dot{d}_b(x,t) + vr'(x)\right] + k_v\left[d_b(x,t) + r(x)\right]\right\}_{x=vt} \quad (4)$$

where m_v, k_v, c_v are the mass, stiffness and damping of the vehicle, respectively; $d_v(t), \dot{d}_v(t), \ddot{d}_v(t)$ are the vertical displacement, velocity and acceleration of the vehicle, respectively; $d_b(x,t), \dot{d}_b(x,t)$ are the vertical displacement and velocity of the bridge at the contact point *x* and time *t*; $r(x)$ is the road surface roughness function with $r'(x) = dr(x)/dx$.

The right-hand-side (RHS) of Eq. (4) can be rewritten as

$$f(t) = \left\{c_v\left[\dot{d}_b(x,t) + vr'(x)\right] + k_v\left[d_b(x,t) + r(x)\right]\right\}_{x=vt} \quad (5)$$

With the Duhamel's integral, the dynamic response of the vehicle can be obtained as

$$d_v(t) = h_v(t) \otimes f(t) \quad (6)$$

where $h_v(t)$ is the impulse response function of the vehicle system. $\otimes$ is the convolution operator.

Ignoring the effect of the road surface roughness and the vehicle damping and submitting Eqs. (2) and (5) into (6), the vehicle response can be written as

$$d_v(t) = h_v(t) \otimes \{k_v[\sum_{i=1}^{N} \phi_i(vt)\, Y_i(t)]\} \quad (7)$$

which is the convolution of the impulse response function and the bridge response and it includes the vehicle and bridge response components. The vehicle response becomes more complicated when the vehicle damping and the road surface roughness are considered, and there is a need of an effective tool to extract the bridge response components from the vehicle response.

Drive by blind modal identification using singular spectrum analysis

The drive by blind modal identification with SSA mainly consists of two steps: the first step is to decompose the vehicle response into a set of independent time series data. The second step is to extract the modal responses through the BSS for the identification of the bridge modal frequencies. Only the dynamic response measurement of the vehicle when crossing the bridge deck is used in the identification.

Decomposition of the vehicle response using SSA

In this step, the single-channel measured vehicle response is decomposed into a multi-channel dataset using SSA. There are two stages for performing the SSA, i.e. decomposition and reconstruction. The first stage is to decompose the time series into a set of elementary matrices based on two separate steps: embedding and singular value decomposition. The second stage is to extract its constituting components based on the diagonal averaging and grouping steps. The SSA adopted in this study is briefly described below whereas more details can be referred to Liu et al.(2014).

1) Embedding

A measurement data vector $\mathbf{d}_v(t) = [d_0, d_1, d_2, \ldots, d_{N-1}]$ with length N can be divided into L lagged vectors X_i as $\{X_i = [d_{i-1}, d_i,\ d_{i+1} \cdots d_{i+N_L-2}]^T,\ \ i = 1,2, \ldots L\}$. N_L is the window length that is an integer between 1 and N, and $L = N - N_L + 1$. These L vectors can further be formed into a trajectory matrix $\mathbf{X}$ as

$$\mathbf{X} = [\mathbf{X}_1, \mathbf{X}_2, \cdots \mathbf{X}_L\ ] = \begin{bmatrix} d_0 & d_1 & \cdots & d_{L-1} \\ d_1 & d_2 & \cdots & d_L \\ \vdots & \vdots & \ddots & \vdots \\ d_{N_L-1} & d_{N_L} & \cdots & d_{N-1} \end{bmatrix} \tag{8}$$

The $(i,j)th$ element of $\mathbf{X}$ in Eq. (8) is $x_{ij} = d_{i+j-2}$. Hence the trajectory matrix $\mathbf{X} \in R^{N_L \times L}$ is a Hankel matrix.

2) Singular value decomposition

Let $\mathbf{S} = \mathbf{X}\mathbf{X}^T$ which is a $N_L \times N_L$ square matrix. N_L eigenvalues and the corresponding eigenvectors of matrix $\mathbf{S}$ are denoted as $\lambda_1, \lambda_2, \ldots, \lambda_{N_L}$ $(\lambda_1 > \lambda_2 > \cdots > \lambda_{N_L})$ and $\mathbf{U}_1, \mathbf{U}_2, \ldots, \mathbf{U}_{N_L}$, respectively. Supposing N_s is the number of positive eigenvalues $(N_s \leq N_L)$, the squared root of these eigenvalues, i.e. $\sqrt{\lambda_1}, \sqrt{\lambda_2}, \ldots, \sqrt{\lambda_{N_s}}$, are referred to as the singular values of the trajectory matrix $\mathbf{X}$. The extremely small singular values are ignored in the decomposition process and it will not affect the accuracy. The elementary matrix $\mathbf{X}_{si}$ for a $\sqrt{\lambda_i}$ can be obtained as

$$\mathbf{X}_{si} = \sqrt{\lambda_i}\mathbf{U}_i\mathbf{V}_i^T \tag{9}$$

where $\mathbf{V}_i = \mathbf{X}^T\mathbf{U}_i/\sqrt{\lambda_i}$. $\mathbf{U}_i$ and $\mathbf{V}_i$ are the left and right singular vectors, respectively. The trajectory matrix $\mathbf{X}$ can then be expressed as the summation of the N_s elementary matrices as

$$\mathbf{X} = \mathbf{X}_{s1} + \mathbf{X}_{s2} + \cdots + \mathbf{X}_{sN_s} \tag{10}$$

The trajectory matrix $\mathbf{X}$ is then decomposed into N_s elementary matrices of rank 1 with a norm equal to the singular value. This is the singular value decomposition of the trajectory matrix **X**.

3) Grouping

All elementary matrices obtained in the last step can be put into N_g groups by a pre-set criteria. The grouping criteria depends on the expected function of the SSA, e.g., denoising, smoothing, harmonic component extracting, etc. The elementary matrices in the same group are summed and N_g resultant matrices, i.e. $\mathbf{X}_{\mathrm{g}1}, \mathbf{X}_{\mathrm{g}2}, \ldots \mathbf{X}_{\mathrm{g}N_\mathrm{g}}$, can be obtained. The original trajectory matrix **X** can then be expressed as

$$\mathbf{X} = \mathbf{X}_{\mathrm{g}1} + \mathbf{X}_{\mathrm{g}2} + \cdots + \mathbf{X}_{\mathrm{g}N_\mathrm{g}} \tag{11}$$

The groups can be formed based on the information contained into the singular vectors (Hassani, 2007). Since the singular values are arranged in a descending order, the first few elementary matrices contribute more than other ones in the trajectory matrix. Therefore each major elementary matrix will form one group for the reconstruction in the proposed method.

4) Skew diagonal averaging

Each resultant matrix in the last step is converted into a new set of time-series data with the same length as the original dataset. A skew diagonal averaging procedure is adopted to recover the time series. Let **Y** be any of the resultant matrixes $\mathbf{X}_{gl}$, with the elements denoted as $y_{ij}, i = 1, 2, \ldots, N_L,\ j = 1, 2, \ldots, L$. For$N_L < L$, the recovered time-series data $\mathbf{d}^{(l)} = [d_0^{(l)}, d_1^{(l)}, \ldots d_{N-1}^{(l)}]$ is given by

$$d_k^{(l)} = \begin{cases} \frac{1}{k+1}\sum_{m=1}^{k+1} y_{m,k-m+2} & \text{for } 0 \le k < N_L - 1 \\ \frac{1}{N_L}\sum_{m=1}^{N_L} y_{m,k-m+2} & \text{for } N_L - 1 \le k \le L \\ \frac{1}{N-k}\sum_{m=k-L+2}^{N-L+1} y_{m,k-m+2} & \text{for } L < k \le N-1 \end{cases} \tag{12}$$

For $N_L > L$, the length N_L should be switched with L in the preceding expressions. There are N_g sets of time series data $\{\mathbf{d}^{(l)},\ l = 1,2, \ldots N_\mathrm{g}\}$ obtained from $\mathbf{d}_v(t)$ and the new data vector $\mathbf{d}(t)$ after the SSA becomes $\mathbf{d}(t) = \sum_{l=1}^{N_\mathrm{g}} \mathbf{d}^{(l)}$.

Blind modal identification with SSA

The multi-channel dataset from SSA is used as the input into the BSS for modal parameter identification. Supposing the dataset includes N_g sets of time series data $\mathbf{d} = \left\{\mathbf{d}^{(l)},\ l = 1,2,\ldots,N_g\right\}^T$. Each set of time series data $\mathbf{d}^{(l)}$ is a linear mixture of n components $\{\mathbf{s}_i,\ i = 1,2,\ldots,n\}$. The relation between the components and the measured data can be written as

$$\mathbf{d} = \mathbf{A}\mathbf{s} \tag{13}$$

where $\mathbf{A}$ is the $N_g \times n$ mixing matrix, $\mathbf{s} = \{\mathbf{s}_1, \mathbf{s}_2, \cdots, \mathbf{s}_n\}^T$ and $\mathbf{d} = \{\mathbf{d}^{(1)}, \mathbf{d}^{(2)}, \cdots, \mathbf{d}^{(N_g)}\}^T$, and both $\mathbf{A}$ and $\mathbf{s}$ are unknown.

Assuming the components $\mathbf{s} = \{\mathbf{s}_1, \mathbf{s}_2, \cdots, \mathbf{s}_n\}^T$ are statistically independent, they can be determined by the second-order blind identification (SOBI) for the over-determined case of ($N_g > n$) as (Belouchrani et al., 1997)

$$\mathbf{s} = \mathbf{W}\mathbf{d} \tag{14}$$

where, the de-mixing matrix $\mathbf{W}$ is the inverse of the mixing matrix $\mathbf{A}$, and it needs to be estimated. There are two steps in the SOBI algorithm: data whitening and the mixing and de-mixing matrices' estimation. For the observed data $\mathbf{d}(t)$, the time-shifted covariance matrix can be written as $\boldsymbol{R}_d(\tau) = E\{\boldsymbol{d}(t)\boldsymbol{d}(t+\tau)^T\}$. The eigenvalue decomposition of $\mathbf{R}_d(0)$ can be computed as $\mathbf{R}_d(0) = \mathbf{E}\mathbf{D}\mathbf{E}^T$, where $\mathbf{E}$ is the orthogonal matrix of eigenvectors and $\mathbf{D}$ is the diagonal matrix of eigenvalues. The whitening matrix $\mathbf{W}_m$ is then calculated (Belouchrani et al., 1997) as

$$\mathbf{W}_m = \mathbf{D}^{-1/2}\mathbf{E} \tag{15}$$

where the observed data $\mathbf{d}$ is whitened to form the whitened data vector which has a unitary covariance matrix. The whitened data is then computed as $\mathbf{z} = \mathbf{W}_m\mathbf{d}$ with $E\{\mathbf{z}\mathbf{z}^T\} = \mathbf{I}$ (McNeill and Zimmerman, 2008). A matrix $\boldsymbol{\Psi}$ that approximately diagonalizes several time-shifted covariance matrices can be obtained using the joint approximate diagonalization (JAD) technique (Belouchrani et al., 1997). The de-mixing and mixing matrices can then be computed as

$$\mathbf{W} = \mathbf{\Psi}^T \mathbf{W}_m \tag{16a}$$

$$\mathbf{A} = \mathbf{W}_m^{-1} \mathbf{\Psi} \tag{16b}$$

The dynamic responses of the vehicle $\mathbf{d}_v$ in Eq. (7) can then be expressed as

$$\mathbf{d}_v = \mathbf{\Phi q} \tag{17}$$

where $\mathbf{q}$ is the vector of vibration modes, and the modal matrix $\mathbf{\Phi}$ equals to the mixing matrix $\mathbf{A}$ in Eq. (16b). The modal responses can be estimated similar to Eq. (14) using BSS as

$$\mathbf{q} = \mathbf{\Phi}^{-1} \mathbf{d}_v \tag{18}$$

where $\mathbf{\Phi}^{-1}$ equals to the de-mixing matrix $\mathbf{W}$ in Eq. (16a).

McNeill and Zimmerman (2008) proposed a framework for the blind modal identification with application of the SOBI algorithm on an expanded and pre-treated dataset. This helps to improve the quality of the estimated modal responses. This framework is adopted in this study for the blind modal identification. The measured data, denoted as $\mathbf{d}_0$, is supplemented by 90° phase shifted data, $\mathbf{d}_{90}$, to double the size of the estimation problem as

$$\begin{bmatrix} \mathbf{s}_0^{(n\times 1)} \\ \mathbf{s}_{90}^{(n\times 1)} \end{bmatrix} = \mathbf{W}^{(2n\times 2N_g)} \begin{bmatrix} \mathbf{d}_0^{(N_g\times 1)} \\ \mathbf{d}_{90}^{(N_g\times 1)} \end{bmatrix} \tag{19}$$

where $\mathbf{s}_{90}$ are the 90° phased shifted components of $\mathbf{s}_0$. The modal responses can be obtained as

$$\mathbf{q} = \frac{1}{\sqrt{2}} [\mathbf{s}_0 + \mathbf{s}_{90}] \tag{20}$$

For a linear vehicle-bridge system, the dominant vehicle or bridge frequencies in the Fourier spectrum of the response component can be identified by curve-fitting. For a nonlinear system, Hilbert transform (HT) could be used to estimate the instantaneous frequency and damping from $\mathbf{q}(t)$ (McNeill and Zimmerman, 2008).

Drive by blind modal identification

The step-by-step procedure of the proposed method is listed as follows:

1) The single-channel measurement of the vehicle response $\mathbf{d}_v(t)$ is separated into a multi-channel dataset $\mathbf{d} = \{\mathbf{d}^{(l)},\ l = 1,2, \ldots N_g\}$ using SSA based on Eqs. (8) to (12). The dataset is denoted as $\mathbf{d}_0$.

2) The dataset is phase-shifted with $90°$ to get the supplement dataset, $\mathbf{d}_{90}$. It is combined with $\mathbf{d}_0$ to form an expanded set of observed data $\mathbf{d}(\mathbf{t}) = \begin{bmatrix} \mathbf{d}_0 \\ \mathbf{d}_{90} \end{bmatrix}$.

3) The whitening matrix $\mathbf{W}_m$ is computed from Eq. (15). The whitened data $\mathbf{z} = \mathbf{W}_m\mathbf{d}(t)$. The joint diagonalizer $\mathbf{\Psi}$ can be obtained by applying the JAD technique to the whitened data $\mathbf{z} = \mathbf{W}_m\mathbf{d}$. Then the de-mixing matrix $\mathbf{W}$ and the mixing matrix $\mathbf{A}$ can be obtained from Eq. 16.

4) The components $\mathbf{s}_0, \mathbf{s}_{90}$ are then obtained based on Eq. (19).

5) The modal responses $\mathbf{q}$ are estimated from Eq. (20). The bridge modal frequencies are obtained from the modal responses.

The flow chart of the proposed method is shown in Figure 2.

Numerical examples

Numerical simulations are performed with the following parameters of the bridge deck: $L = 30m, \rho = 1000\,kg/m$, $I = 0.175m^4, E = 27.5GPa$. The first two natural frequencies of the deck are 3.83 and 15.32 Hz, respectively. The properties for the vehicle are: $m_v = 200kg, k_v = 170\,kN/m$. The vehicle modal frequency is 4.64Hz. Damping of the bridge and vehicle are not considered in this study. The moving speed of the vehicle is constant at $2.0\,m/s$ and the time step is set as 0.001s in the simulation. Class A road surface roughness is used (ISO 8606). Ongoing traffic is modeled as white-noise excitation at supports of the deck with an amplitude of 0.02m/s^2. These parameters are used for all numerical studies in this paper unless otherwise stated. The dynamic response of the vehicle and its frequency spectrum are presented in Figure 3. It is noted that only the vehicle frequency is clearly noted in the spectrum whereas the bridge frequencies cannot be identified.

Selection of the window length

The window length is one of the most important parameters in the SSA technique and it has a large effect on the decomposition (Harmouche et al., 2018). There are some recommendations on the selection of window length (Golyandina, 2010; Hassani et al., 2011). A larger value of L makes longer period oscillations to be solved, but too large value may involve a large number of eigentriples and miss some important principal components with high contributions. Although lots of trail applications and various methods have been discussed for the selection of optimal values of L, there is still a lack of theoretical regulation for window length choosing. In this paper, three typical values from small to large are selected to show the effect of the window length.

The dynamic response of the vehicle contains information of both the vehicle and bridge, and the first two bridge modes and one vehicle mode are targeted components for extraction. The unsupervised component grouping method based on hierarchical clustering is adopted for the automatic selection of the elementary matrices to compose the desired dataset from the vehicle response (Harmouche et al., 2018). Each elementary matrix is used as one group and it does not need the grouping selection. In the following sections, the time series data with the top 20 percent of eigenvalues reconstructed from the SSA are adopted as input to the BSS to estimate the three targeted components.

Three different window lengths, i.e. 100, 500 and 1000, are selected for the study. The first three time series data and their spectra from the SSA decomposition are presented in Figure 4. The frequency of the first time series data for all window lengths is 4.73Hz and it is very close to the vehicle frequency 4.64Hz. The second time series data from 500 and 1000 window lengths has only one distinct peak at 3.73 Hz which is close to the first bridge mode at 3.83Hz. The amplitude of the time series data is much larger from using 1000 window length. When the window length is 100, there are two close peaks which are believed to be the bridge frequency and the vehicle modal frequency. Neither the vehicle or bridge modes can be found in the third time series data in Figure 4.

The components decomposed from the BSS are presented in Figure 5. The components corresponding to the vehicle and bridge modal frequencies are noted clearly separated for all window lengths, and the larger window length can provide better separation results. The third component in Figure 5 is related to the second bridge modal frequency 15.32Hz which has becomes more notable compared to that noted directly from the SSA method. The proposed method is noted less sensitive to the effect of window length and the bridge modal frequencies can better be isolated than by simply application of the SSA only. The window length is selected to be 1000 in the following studies.

The effect of road surface roughness

The road surface roughness has significant effect on the indirect bridge modal identification. Figure 6 shows the vehicle response and its corresponding spectrum when the road surface roughness is Class B. There is only one peak in Figure 6(b) at 4.67Hz which is close to the vehicle mode at 4.64Hz and the bridge mode cannot be identified from the spectrum. Figure 7 shows the first two components from the proposed method. The first bridge mode can be identified from the peak of the first component in Figure 7(b) as 3.77Hz and the vehicle mode is related to the peak of the second component in Figure 7(b) as 4.67Hz. The proposed method has the capability to separate the components related to the vehicle and first bridge modal frequency even when the road surface roughness is Class B.

Effect of vehicle parameters

Effect of vehicle mass

Three different vehicle masses, i.e. 200kg to 500kg and 1000kg are investigated with the vehicle speed 2.0 m/s. Other parameters are the same as those stated earlier. The vehicle modal frequencies are 4.64Hz, 2.93Hz and 2.08Hz respectively for vehicles with different masses described above. Figure 8 shows the identified first three response components and their frequency spectra. The frequencies of the first components in Figure 8(a) are 3.77Hz, 2.90Hz and 2.03Hz for vehicle masses 200kg, 500kg and 1000kg, respectively. The latter two frequencies correspond to the vehicle frequency. The first frequency corresponds to the frequency of the first bridge mode. The corresponding vehicle mode at 4.70Hz is noted in the second component as shown in Figure 8(b). The first bridge modal frequency is noted in the second components in Figure 8(b) for the 500kg and 1000kg mass vehicles as 3.90Hz and 3.83Hz respectively. These results show that more accurate modal frequency can be obtained with a heavier vehicle. Figure 8(c) shows the third response component and the peak frequency is around 15.27Hz corresponding to the second bridge mode. In comparing the spectrum of the bridge related components, it is noted that the spectrum amplitude increases with the vehicle mass. This may suggest that a heavier testing vehicle may amplify the bridge vibration, which is beneficial for the drive-by bridge modal frequency identification.

Effect of vehicle stiffness k_v

A moderate vehicle mass 500kg is selected with the vehicle stiffness of 340kN/m, 680kN/m and 1360kN/m respectively and a vehicle speed of 2.0m/s. The corresponding vehicle modal frequencies are 4.15, 5.87, and 8.30Hz, respectively. Figure 9 shows the components of the responses and their spectra with different stiffness values. The peak frequencies are 3.77Hz and 15.43Hz in Figures 9(a) and 9(c) and they are related to the first and second bridge modes. Figure 9(b) shows the three frequencies i.e. 4.33Hz, 5.90Hz and 8.20Hz which correspond to the vehicle mode with different stiffness respectively. These results show that the vehicle stiffness does not have a large effect on the identified results.

Effect of vehicle speed

The vehicle parameters are selected as $m_v = 500kg$, $k_v = 170kN/m$ while other parameters remain the same as those stated earlier. The vehicle frequency is 2.90Hz. The vehicle speeds 2.0m/s, 4.0m/s and 8.0m/s are studied. Figure 10 presents the decomposed components and their spectra. Figure 10(a) shows the first component with a frequency at around 2.90Hz for all vehicle speeds. Figures 10(b) and 10(c) are the second and third components with frequencies at 3.87Hz and 15.27Hz respectively. These two frequencies correspond to the first and second bridge modal frequencies. Since the frequency resolution is increased with a lower speed as the time record length for the vehicle moving on the deck is increased, the accuracy of identified frequency can be improved with a lower vehicle speed. A moderate vehicle speed is therefore recommended when identifying higher order modal frequencies.

Effect of measurement noise

Practical measurement is always contaminated with noise. White noise is added to the calculated acceleration response to simulate the polluted measurement as,

$$acc_m = acc_{cal} + E_p * N_{oise} * \sigma(acc_{cal}) \tag{21}$$

where acc_{cal} is the calculated acceleration response; E_p is the Noise Level; N_{oise} is a vector of random values with zero mean and unit variance; and $\sigma(acc_{cal})$ is the standard deviation of the calculated acceleration response.

The vehicle speed is 4.0m/s and other parameters are the same as those in the last subsection. Three different noise levels, i.e. 5%, 10% and 20%, are simulated. Figure 11 shows the identified results. The identified response components and spectra at different noise levels are close together indicating that the proposed method is insensitive to measurement noise. This is mainly due to the fact that only the first 20 percent SSA components are adopted as the input to BSS to get the first three targeted components of BSS. SSA components with low singular values have been removed to reduce the white noise effects.

Identification of the instantaneous frequencies for the VBI system using proposed method

The vehicle is noted to be can also be used as an actuator to excite the bridge structure and the vehicle-induced vibration is a kind of non-stationary process (Kim et al., 2014). Hilbert Transform (HT) may be used to extract instantaneous frequencies of the VBI system in the indirect bridge modal identification. The vehicle parameters are selected as $m_v = 1000kg, k_v = 170kN/m$ and other parameters are the same as those stated earlier. The natural frequency of the vehicle is 2.08Hz. The dynamic response and the spectrum of the vehicle are given in Figure 12. There are two peaks in the spectrum, and the first peak corresponds to the vehicle mode at 2.07Hz and the second one is related to the first bridge mode at 3.87Hz. The first and second response components are shown in Figure 13(a) and the corresponding instantaneous frequencies obtained from HT are presented in Figure 13(b). The average values of the first and second components are 2.08Hz and 3.87Hz which are the vehicle frequency and the first bridge modal frequency respectively. The oscillations at the beginning and end of the instantaneous frequency are due to the Gibbs phenomenon with record length of data. The middle part of the time history oscillates between 3.79Hz and 3.98Hz. Since the vehicle speed is 2.0m/s and the bridge length is 30m, the driving frequency is about 0.07Hz (Yang et al., 2004). This instantaneous frequency is modulated by the driving frequency. The result shows that the driving frequency could also be identified by the proposed method.

Experimental verification

Experimental setup

A vehicle-bridge interaction model was built in the laboratory as shown in Figure 14. The bridge model consists of three rectangular steel beams. The 6m long main beam is in the middle with 100mm width and 15mm depth. It is continuous and symmetrical over a middle support. A 3m leading beam and a 3m trailing beam are sitting in front of and at the rear of the main beam to allow for acceleration and deceleration of the vehicle.

Different configurations of the vehicle model with one and two-axle are built for the study. One-axle vehicle models the quarter vehicle in this paper. An U-shaped aluminium section is glued to the top surface of the beam as direction guide for the vehicle. The model vehicles are pulled along the guide with an electric motor. BeanDevice AX-3D wireless accelerometers are installed on the vehicles to measure the dynamic response during its passage over the deck. They are installed on the vehicle models above the axles as shown in Figure 14(c). Laser sensors are installed along the beam to record the time instants when the vehicles arrive at and exit from the main beam. These time instants are used to calculate the moving speed of the vehicle.

Modal test on the vehicle and bridge models

The modal testing has been carried out on the vehicle and bridge models. 14 accelerometer sensors by PCB Piezotronics are installed evenly on the main beam bridge to measure the dynamic responses, as shown in Figure 14(a) and the impulse hammer is used to excite the beam bridge. The first two natural bridge frequencies are obtained as 5.68, and 8.48 Hz, respectively. The modal testing is also carried out on the single-axle vehicle with the impulse hammer and one accelerometer. The frequency of the single-axle vehicle is 29.37Hz.

Frequency identification using the response of a single-axle vehicle

The vehicle-bridge interaction test was conducted in laboratory using two vehicles as shown in Figure 14(c). The two-axle vehicle simulates the traffic excitation with three different weights. The mass of the vehicle is 4.0, 6.5 and 9.0kg-weight for load cases m1, m2 and m3 respectively.

The single-axle vehicle is used as the mobile sensory system to capture the bridge response. The vehicle is pulled across the beam at three different speeds of 0.10, 0.14 and 0.21m/s and they are referred to as v1, v2 and v3 speeds respectively.

The response of the single-axle vehicle is used to identify the bridge frequencies with the proposed method. The window length for SSA is taken as 500. As the same as the simulation, the time series data with the top 20 percent of eigenvalues are used as the input of BSS.

Figure 15 shows the vehicle response and its spectrum when the speed is 0.10m/s at load case m1. There is a dominate frequency around 30Hz which corresponds to the vehicle modal frequency. The decomposed components using proposed method are presented in Figure 16. The first component has the frequency 5.21Hz that is close to the first modal frequency of the deck. Similarly, the frequency 8.32Hz in Figure 16(b) is related to the second bridge mode. The vehicle modal frequency is identified in the third component as 29.35 Hz.

Figure 17(a) shows the spectra of the decomposed response components with different load cases when the speed is 0.14m/s. Figure 17(b) shows the spectra of the decomposed components under different speeds for load case m2. Table 1 shows the identified results for all the tests considering different speeds and weights. The vehicle-bridge weight ratios are 0.06, 0.09 and 0.13 respectively for the three load cases studied. Results from Figure 17(a) and Table 1 show that the weight of the two-axle vehicle does not have a large effect on the identified results from the response of the single-axle vehicle. It may be concluded that the proposed method is insensitive to the operating traffic excitation. However, Figure 17(b) and Table 1 show that the vehicle speed has a large effect on the identified results. This provides experimental evidence confirming similar observation in the numerical study.

Frequency identification using the responses of a two-axle vehicle

Two wireless accelerometers are also installed on the two-axle vehicle with one sensor on top of the front axle and another one on top of the rear axle. The dynamic responses obtained are shown in Figure 18. The response difference from the two accelerometers is used in the identification. All parameters are the same as those for last study. Figures 19(a) and (b) show the spectra of the first three components with different vehicle speeds and weights respectively. The identified bridge and vehicle frequencies are summarized in

Table 2. The vehicle frequency and the first two bridge modal frequencies can be separately identified. Figure 19(a) and Table 2 show that an increase of the vehicle mass has no obvious effect on the identified bridge frequencies. The identified bridge frequencies in Figure 19(b) show small variation with the vehicle speed. This is mainly due to the reduction of the frequency resolution in the spectrum when the vehicle speed increases.

Time frequency analysis of the bridge response components

The time frequency analysis of the bridge response components using Hilbert transform has also been conducted when the two-axle vehicle moves on the deck with 9kg mass at 0.21m/s. The first two response components and their instantaneous frequencies are shown in Figure 20. There is no large oscillation in the instantaneous frequency time history, and the mean values 5.56Hz and 8.64Hz correspond to the first and second modal frequencies of the bridge.

Conclusions

A drive by blind modal identification method with singular spectrum analysis has been developed to extract the bridge modal frequencies from the dynamic response of a passing vehicle. Numerical and experimental results show that the proposed method is effective and reliable to extract the frequencies. The proposed method is insensitive to the window length in the SSA compared with the direct SSA. The vehicle and bridge modal frequencies can be separated easily with the proposed method even with the Class B road surface roughness. The effect of vehicle parameters on the identification was then investigated numerically. Results show that a heavier vehicle with a lower speed can get more accurate identified frequency, and the vehicle stiffness does have a big effect on the identified results. The proposed method is also robust to measurement noise. Further analysis with the Hilbert Transform shows that the proposed method could be used to identify the instantaneous frequency of the vehicle-bridge interaction system.

Acknowledgements

This research is supported by research funding of the Australian Research Council Discover Project (DP160103197). The financial aids are gratefully acknowledged.

References

Antoni J. (2005) Blind separation of vibration components: Principles and demonstrations. *Mechanocal Systems and Signal Processing*, 19(6): 1166-1180.

Belouchrani A., Abed-Meraim K., Cardoso J.-F. and Moulines E. (1997) A blind source separation technique using second-order statistics. *IEEE Transactions on Signal Processing*, 45(2): 434-444.

Chang K.C., Wu F.B. and Yang Y.B. (2010) Effect of road surface roughness on indirect approach for measuring bridge frequencies from a passing vehicle. *Interaction and multiscale mechanics*, 3(4): 299-308.

Clough R.W. and Penzien J. (1975) *Dynamics of structures*. New York: McGraw-Hill.

Golyandina N. (2010) On the choice of parameters in singular spectrum analysis and related subspace-based methods, *Statistics & Its Interface*, 3(3), 259-279.

Harmouche J., Fourer D., Auger F., Borgnat P. and Flandrin P. (2018) The sliding singular spectrum analysis: a data-driven nonstationary signal decomposition tool. *IEEE Transactions on Signal Processing*, 66(1): 251-263.

Hassani H. (2007) Singular spectrum analysis: methodology and comparison. *Journal of Data Science*, 5(2): 239-257.

Hassani H., Mahmoudvand R. and Zokaei M. (2011) Separability and window length in singular spectrum analysis. *Comptes Rendus Mathematique,* 349(17-18): 987–990.

Hazra B., Roffel A., Narasimhan S. and Pandey M.D. (2010) Modified cross-correlation method for the blind identification of structures. *Journal of Engineering Mechanics ASCE*, 136(7): 889-897.

ISO S. 8608, (1995) *Mechanical Vibration–Road Surfaces Profiles–Reporting of Measured Data*. International Organization for Standardization, Switzerland.

Kerschen G., Poncelet F. and Golinval J.-C. (2007) Physical interpretation of independent component analysis in structural dynamics. *Mechanical Systems and Signal Processing*, 21(4): 3072-3087.

Kim C.-W., Isemoto R., McGetrick P., Kawatani M. and Obrien E.J. (2014) Drive-by bridge inspection from three different approaches. *Smart Structures and Systems*, 13(5): 775-796.

Liu K., Law S.S., Xia Y. and Zhu X.Q. (2014) Singular spectrum analysis for enhancing the sensitivity in structural damage detection. *Journal of Sound and Vibration*, 333(2): 392-417.

Liu K., Law S. S., Zhu X.Q. and Xia Y. (2014) Explicit form of an implicit method for inverse force identification. *Journal of Sound and Vibration*, 333(3): 730-744.

Malekjafarian A., McGetrick P.J. and Obrien E.J. (2015) A review of indirect bridge monitoirng using passing vehicles. *Shock and Vibration*, Article ID 286139.

Malekjafarian A. and Obrien E.J. (2017) On the use of a passing vehicle for the estimation of bridge mode shapes. *Journal of Sound and* Vibration, 397: 77-91.

McNeill S. and Zimmerman D. (2008) A framework for blind modal identification using joint approximate diagonalization. *Mechanical Systems and Signal Processing*, 22(7): 1526-1548.

Poncelet F., Kerschen G., Golinval J.-C. and Verhelst D. (2007) Output-only modal analysis using blind source separation techniques. *Mechanical Systems and Signal Processing*, 21(6): 2335-2358.

Sadhu A., Narasimhan S. and Antoni J. (2017) A review of output-only structural mode identification literature employing blind source separation methods. *Mechanical Systems and Signal processing*, 94: 415-431.

Wang Y and Hao H. (2013) Damage identification scheme based on compressive sensing. *Journal of Computing in Civil Engineering*, 29: 04014037.

Yang Y. and Nagarajaiah S. (2012) Time-frequency blind source separation using independent component analysis for output-only modal identification of highly damped structures. *Journal of Structural Engineering ASCE*, 139(10): 1780-1793.

Yang Y.B., Chang K.C. and Li Y.C. (2013) Filtering techniques for extracting bridge frequencies from a test vehicle moving over the bridge. *Engineering Structures*, 48: 353-362.

Yang Y.B., Li Y.C. and Chang K.C. (2012) Using two connected vehicles to measure the frequencies of bridges with rough surface: a theoretical study. *Acta Mechanica*, 223(8): 1851-1861.

Yang Y.B., Lin C.W. and Yau J.D. (2004) Extracting bridge frequencies from the dynamic response of a passing vehicle. *Journal of Sound and Vibration,* 272(3): 471-493.

Yang Y.B. and Yang J.P. (2018) State-of-the art review on modal identification and damage detection of bridges by moving test vehicles. *International Journal of Structural Stability and Dynamics*, 18(2): 1850025.

Zhen L., Peng D., Yi Z., Xiang Y. and Chen P. (2017) Underdetermined blind source separation using sparse coding. *IEEE transactions on neural networks and learning systems*, 28: 3102-3108.

Zhou W. and Chelidze D. (2007) Blind source separation based vibration mode identification. *Mechanical Systems and Signal Processing*, 21(8): 3072-3087.

Zhu X.Q. and Law S.S. (2002) Dynamic load on continuous multi-lane bridge deck from moving vehicles. *Journal of Sound and Vibration*, 251(4): 697-716.

Zhu X.Q. and Law S.S. (2015) Structural health monitoring based on vehicle-bridge interaction: accomplishments and challenges. *Advances in Structural Engineering*, 18(12): 1999-2015.

List of figures:

Table 1. Bridge and vehicle frequencies from the response of one-axle vehicle

		v1			v2			v3		
		m1	m2	m3	m1	m2	m3	m1	m2	m3
Bridge (Hz)	1^{st}	5.21	5.22	4.93	5.62	5.59	5.55	5.12	5.12	5.09
	2^{nd}	8.31	8.36	8.31	8.50	8.51	8.48	8.54	8.72	8.66
Vehicle (Hz)		29.37	29.40	29.30	29.58	29.56	29.68	29.53	29.39	29.65

Table 2. Bridge and vehicle frequencies from dynamic response of the two-axle vehicle

		v1			v2			v3		
		m1	m2	m3	m1	m2	m3	m1	m2	m3
Bridge (Hz)	1^{st}	4.94	5.30	5.19	5.68	5.64	5.67	5.86	5.41	5.56
	2^{nd}	8.37	8.35	8.35	8.47	8.47	8.47	8.57	8.62	8.64
Vehicle (Hz)		33.79	32.19	32.15	33.92	32.44	31.65	33.33	32.57	32.37

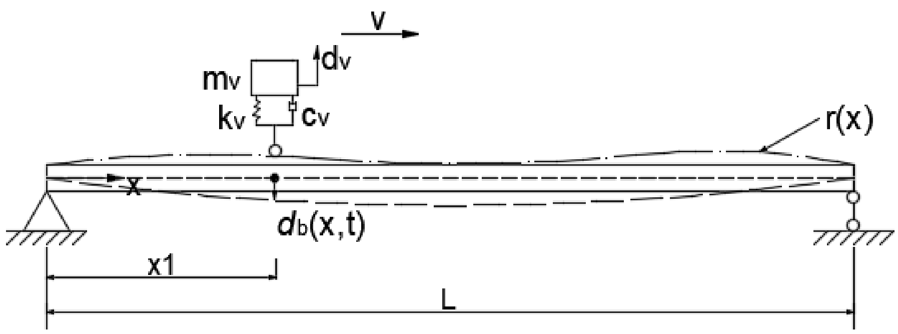

Figure 1 Vehicle-bridge system

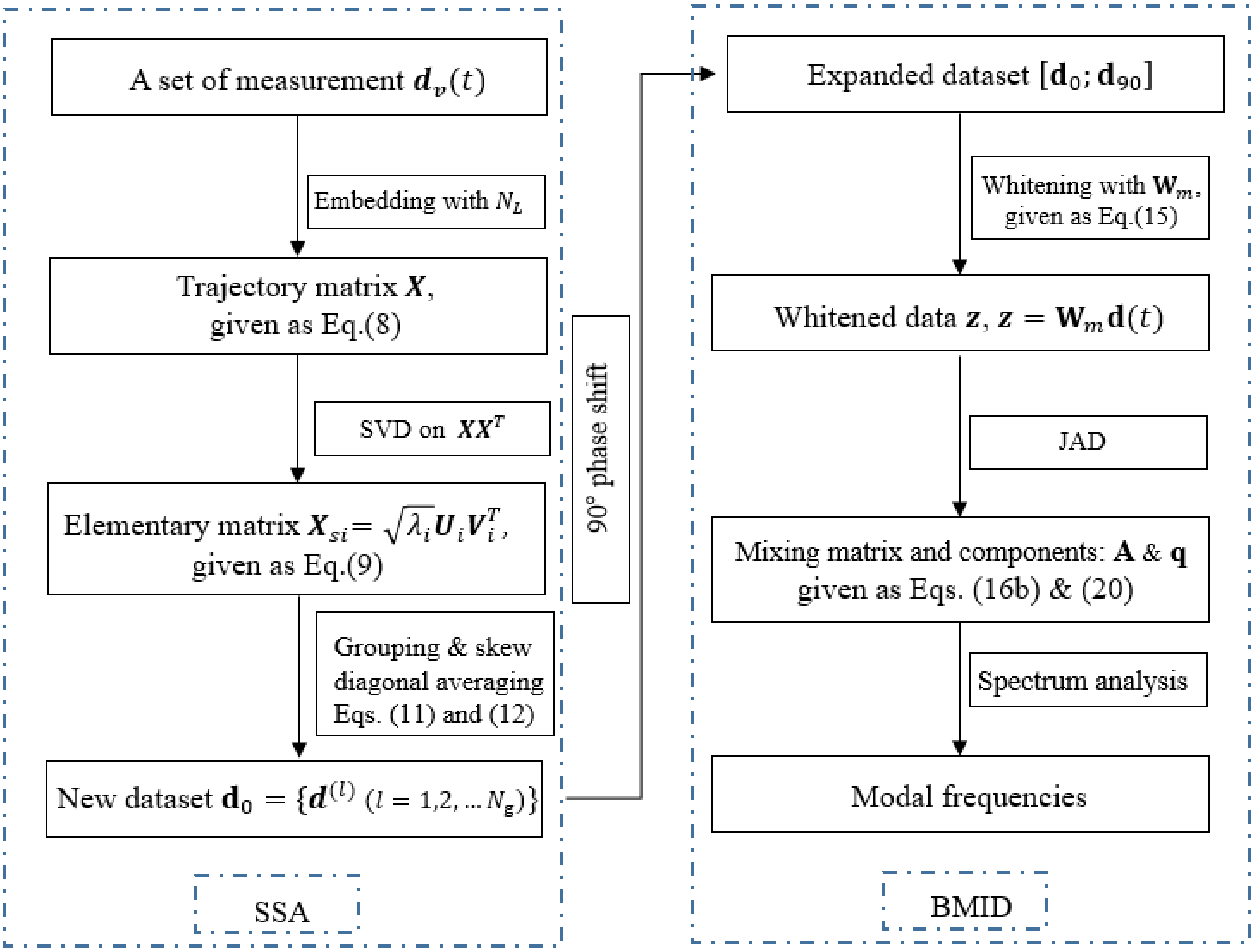

Figure 2 Flow chart of proposed method

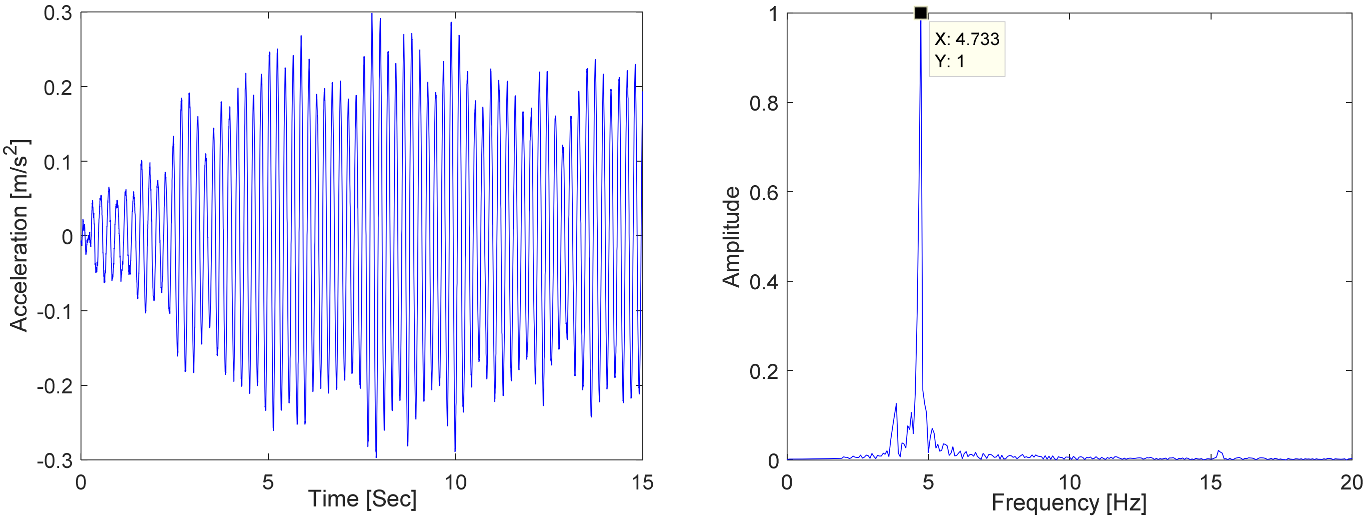

(a) The acceleration response of vehicle (b) The spectrum

Figure 3 Vehicular response and its spectrum when moving on top of bridge deck

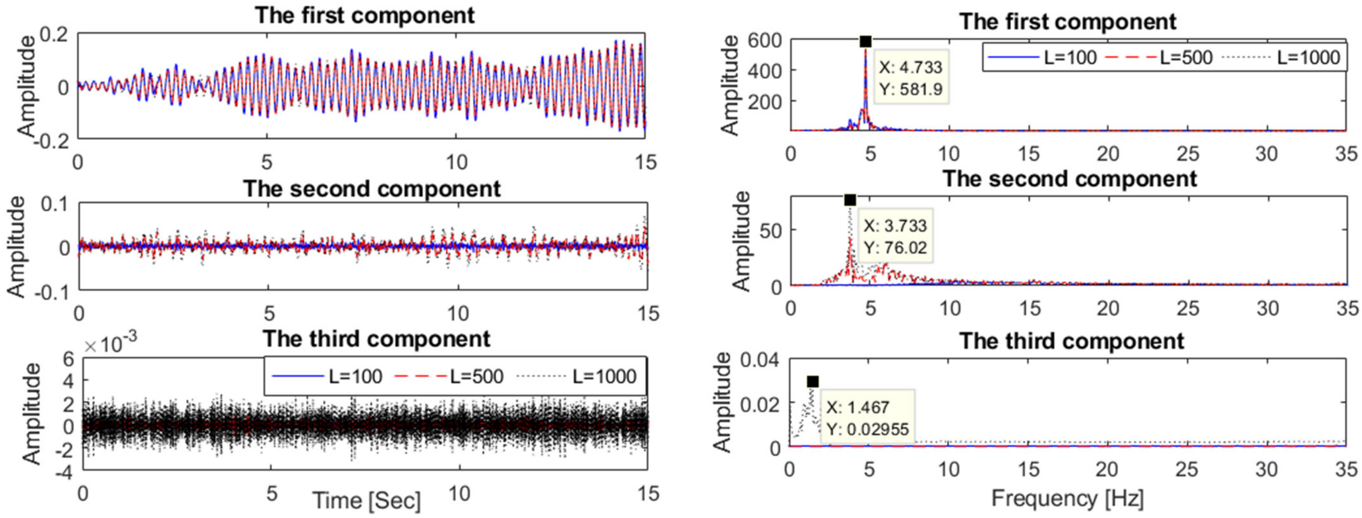

(a) The dataset

(b) Their spectra

Figure 4 Dataset and their spectra by SSA

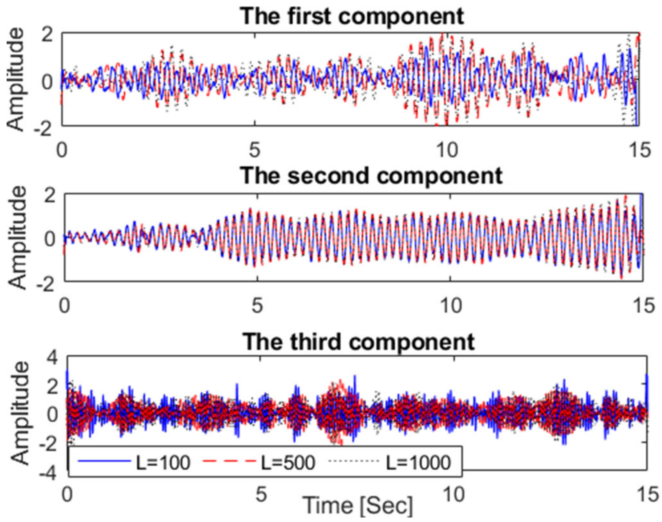

(a) The response components

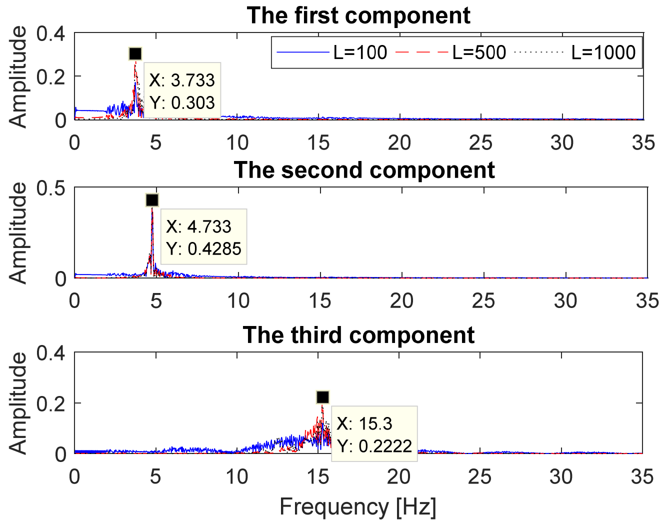

(b) Their spectra

Figure 5 Response components and their spectra by the proposed method

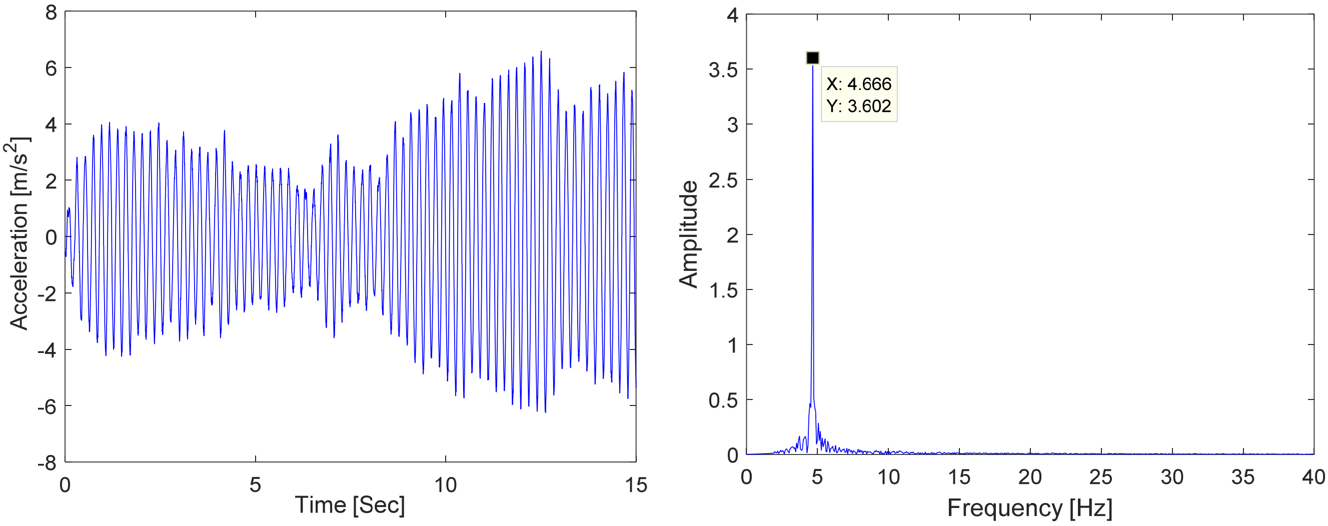

(a) The acceleration response of vehicle (b) The spectrum

Figure 6 Vehicular response and its spectrum for Class B road surface roughness

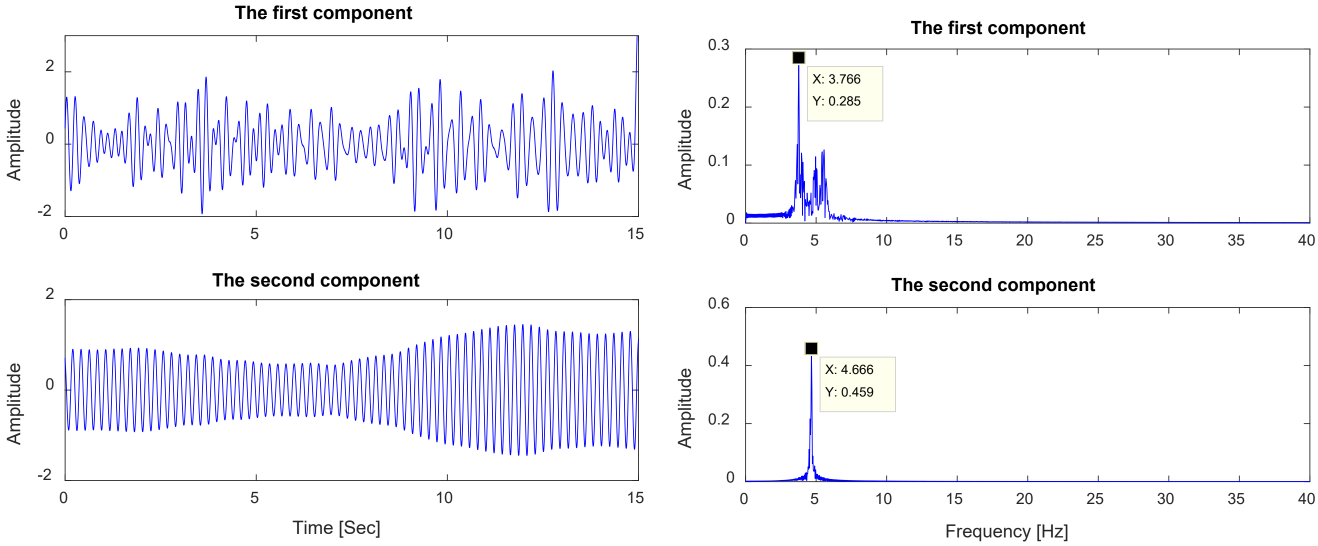

(a) The response components (b) The spectra

Figure 7 The first two components and their spectra by the proposed method

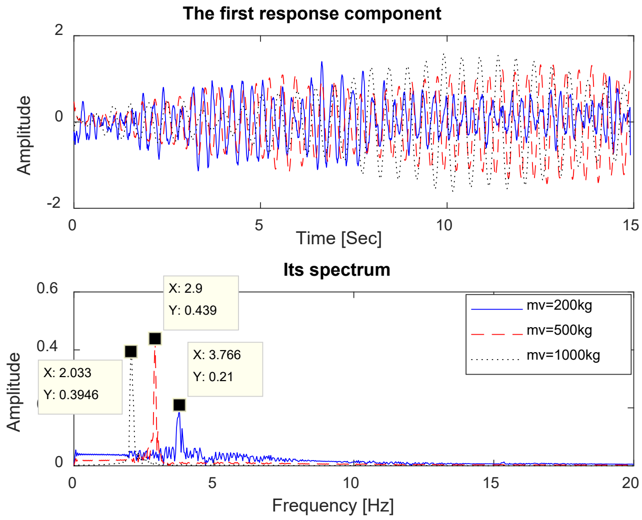

(a) The first response component

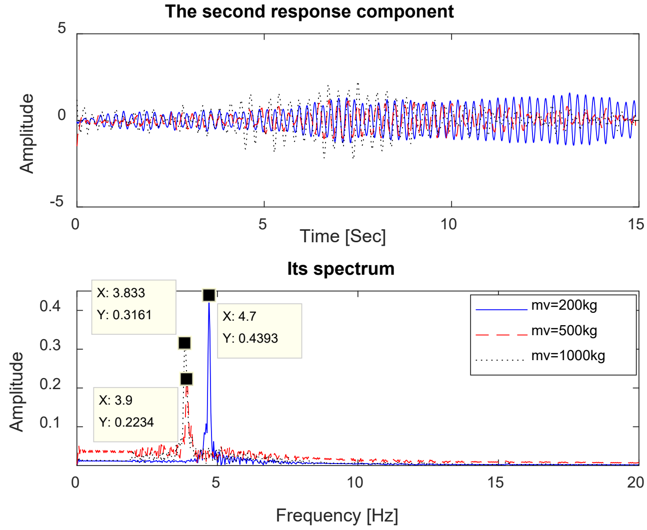

(b) The second response component

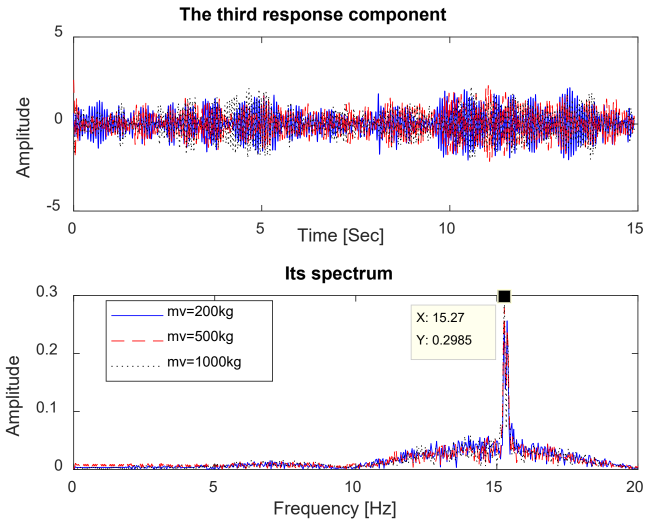

(c) The third response component

Figure 8 Response components and their spectra with different vehicle mass

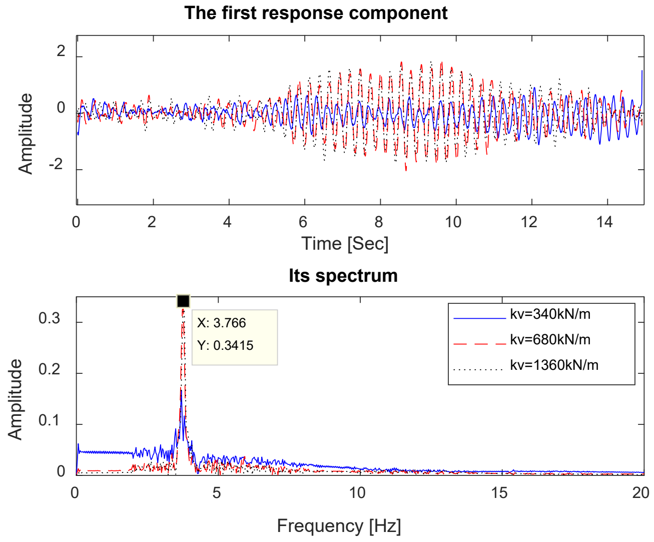

(a) The first response component

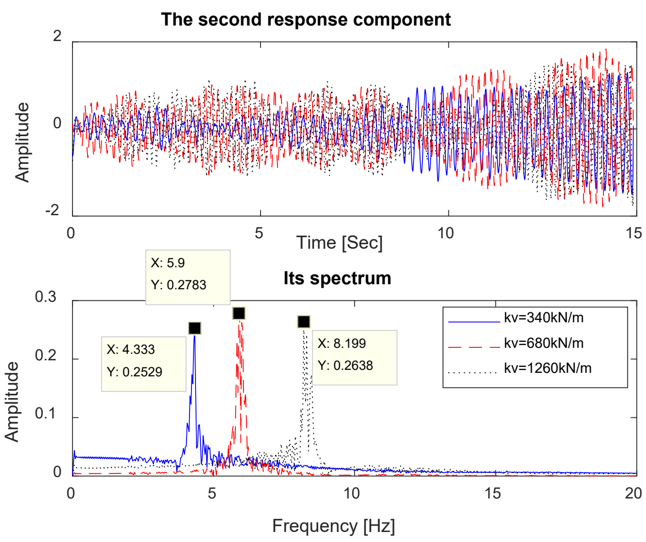

(b) The second response component

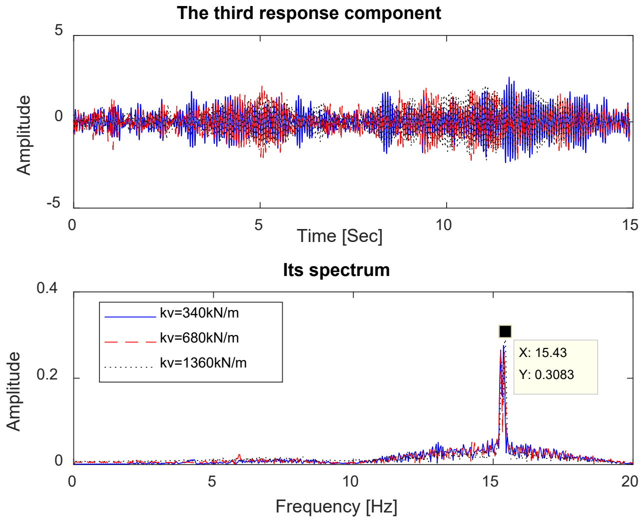

(c) The third response component

Figure 9 Response components and their spectra with different vehicle stiffness

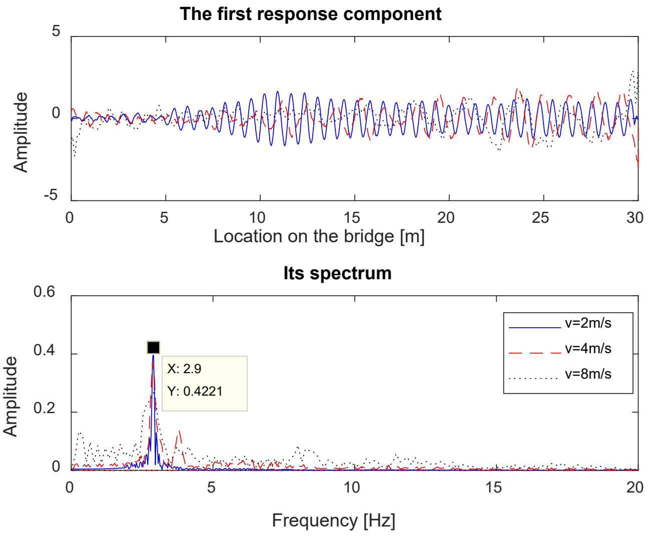

(a) The first response component

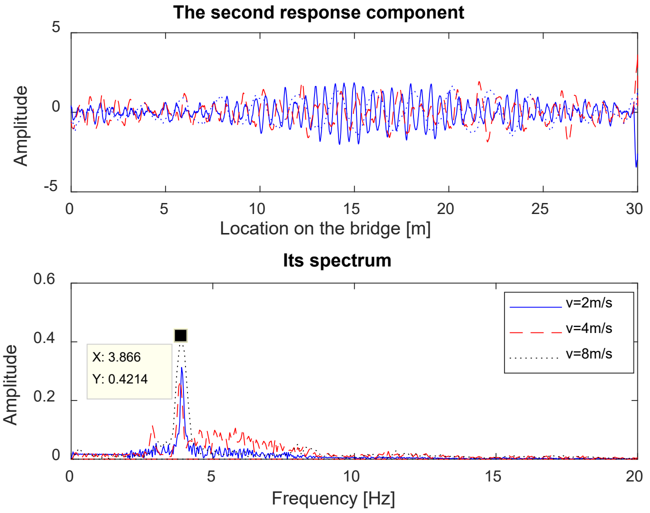

(b) The second response component

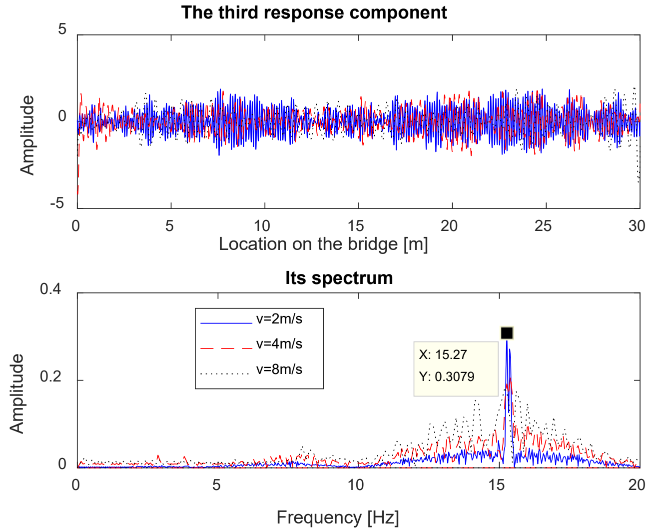

(c) The third response component

Figure 10 Response components and spectra considering different vehicle speed

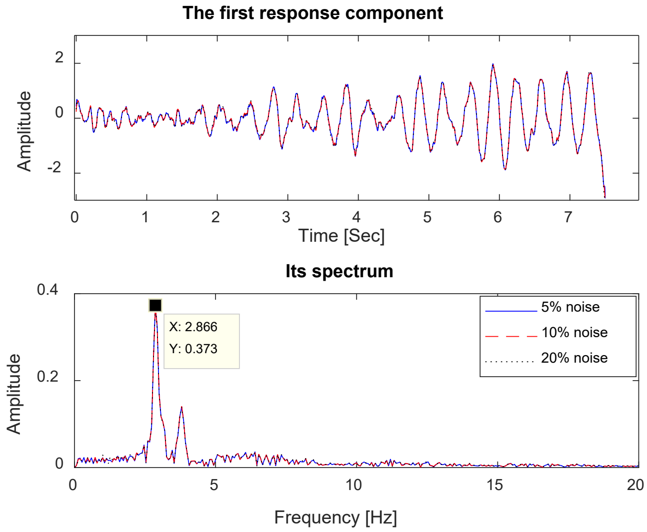

(a) The first response component

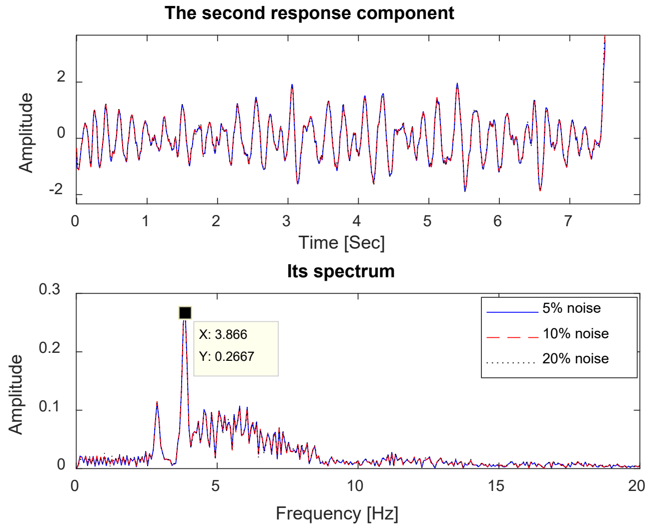

(b) The second response component

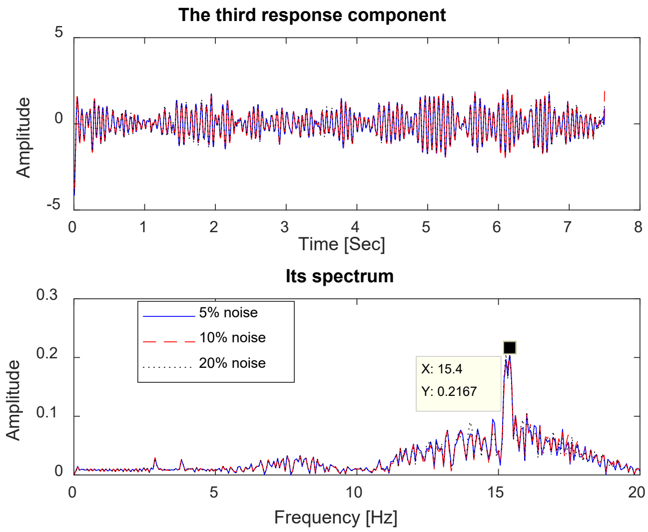

(c) The third response component

Figure 11 Response components and their spectra with different noise levels

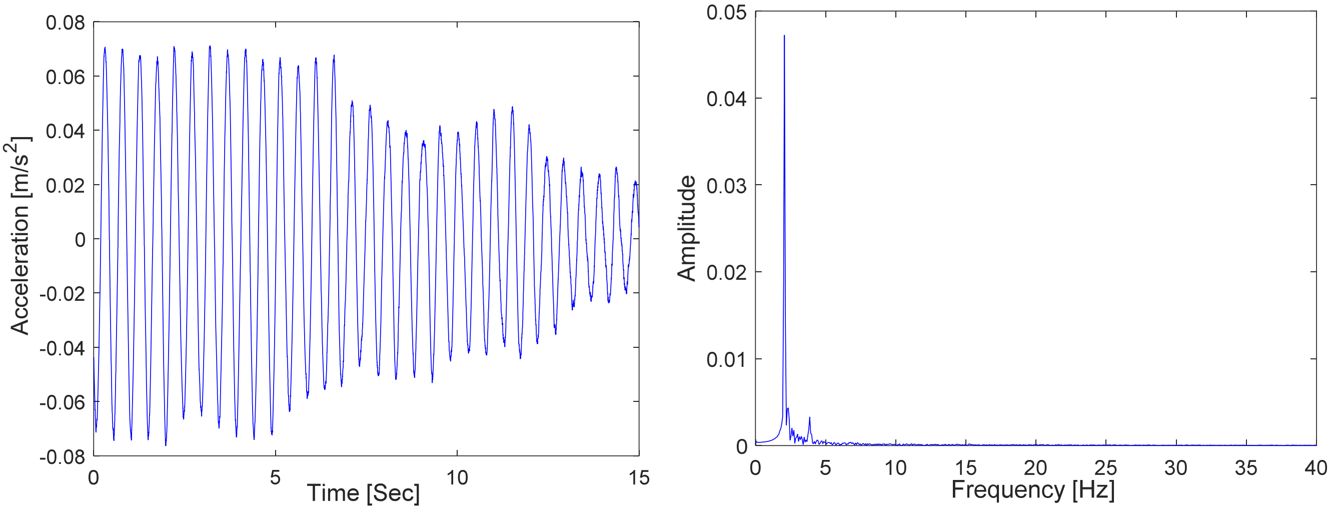

(a) Dynamic response of the vehicle (b) Spectrum of response

Figure 12 Vehicular response and spectrum

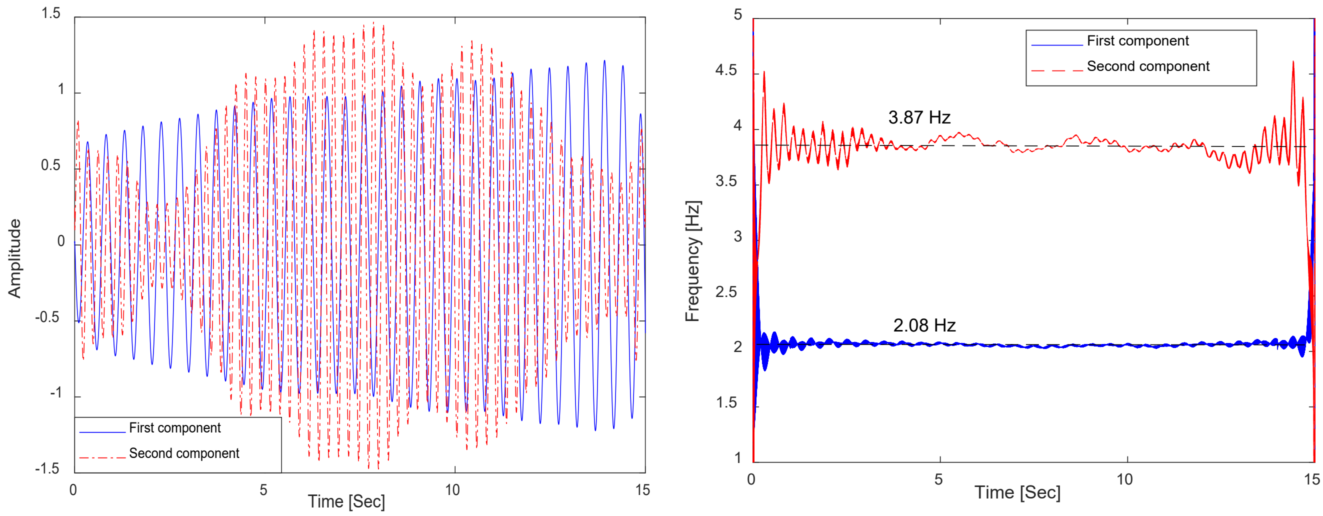

(a) The first two response components (b) The instantaneous frequencies

Figure 13 Vehicular response components and instantaneous frequencies

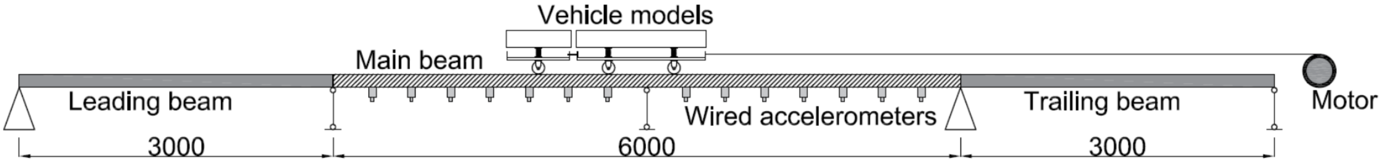

(a) Schematic diagram of the VBI test system in the lab


(b) Photo of the bridge model

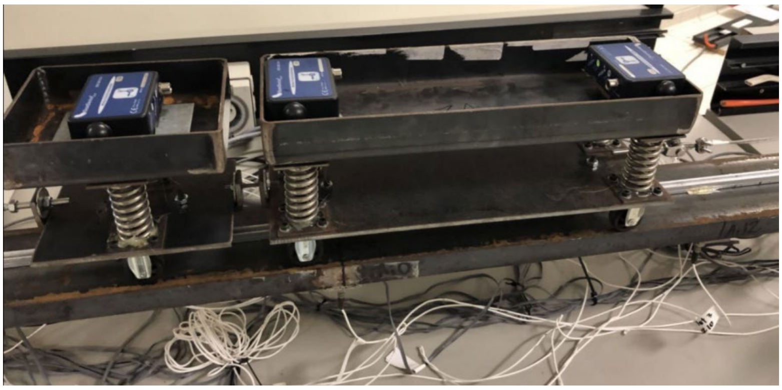
(c) Instrumentation on the vehicle models with wireless sensors

Figure 14 Vehicle-bridge interaction model

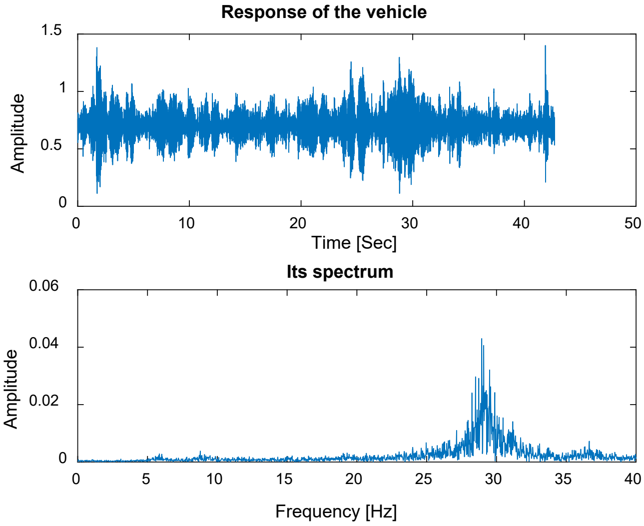

Figure 15 Vehicle response and its spectrum

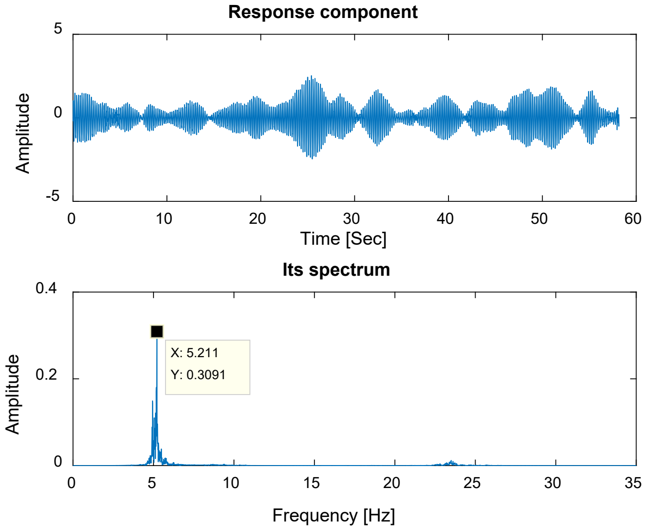

(a) First component and its spectrum

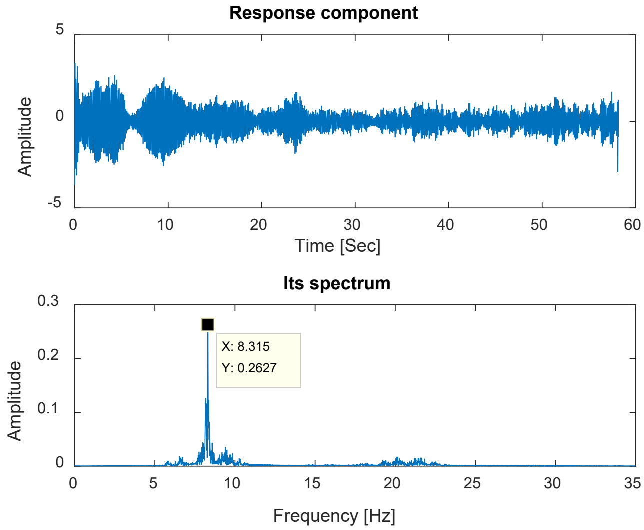

(b) Second component and its spectrum

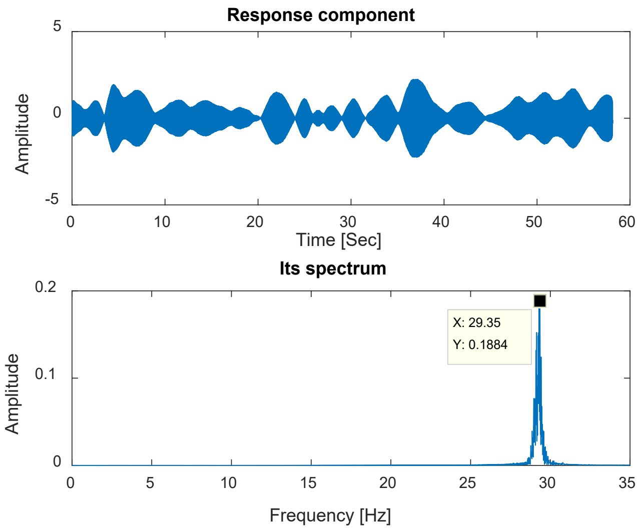

(c) Third component and its spectrum

Figure 16 Decomposed components and their spectra from vehicle response

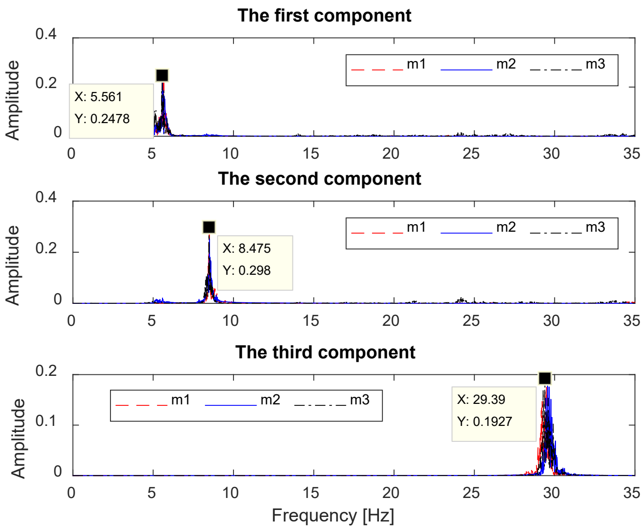

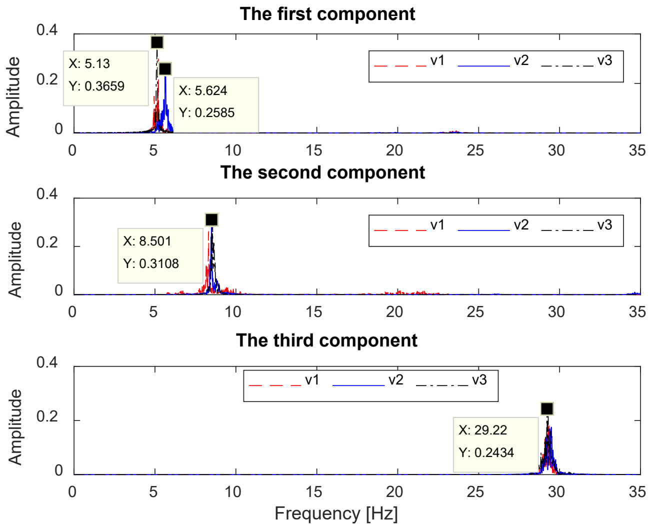

(a) Spectra of the decomposed components consider different weight of two-axle vehicle

(b) Spectra of the decomposed components consider different moving speed

Figure 17 Spectra of the decomposed components under different test conditions

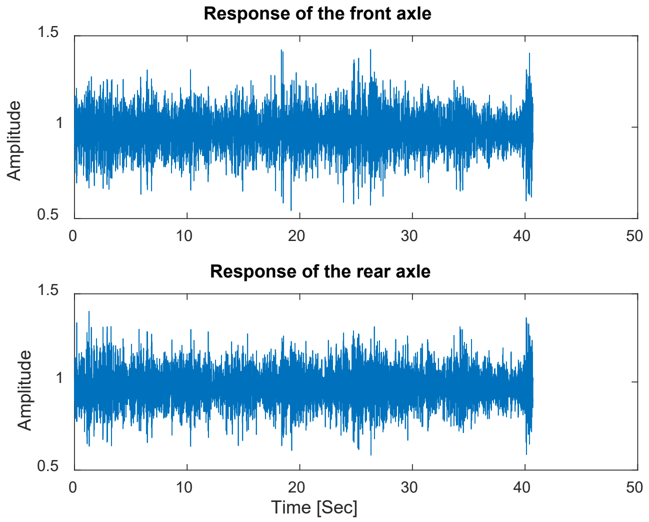

Figure 18 Dynamic responses of the two-axle vehicle

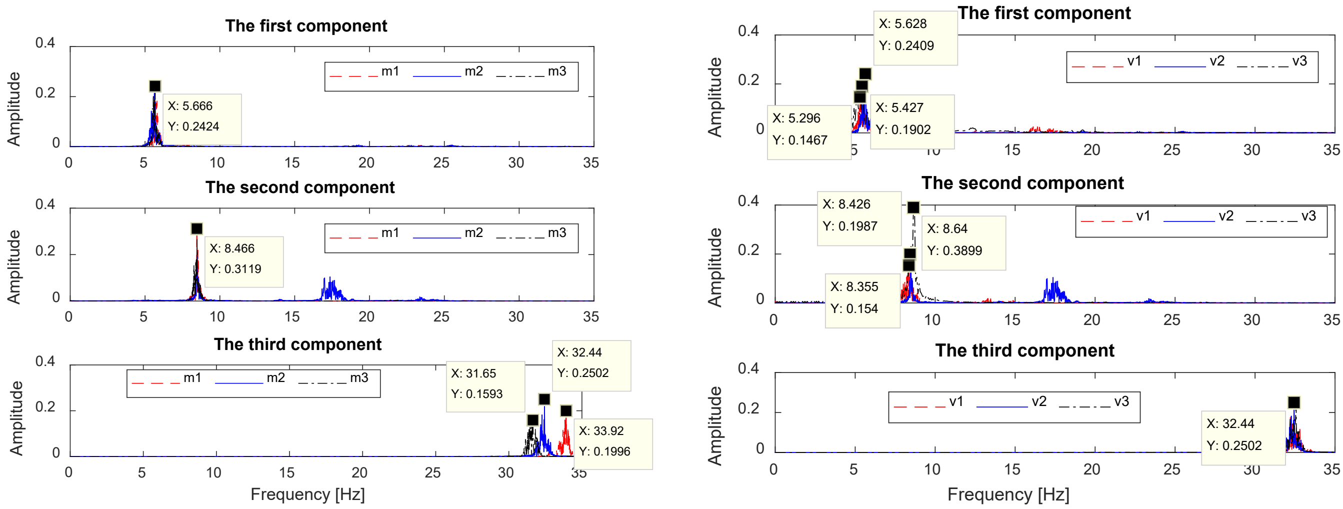

(a) Spectra of the decomposed components consider different weight of two-axle vehicle

(b) Spectra of the decomposed components consider different moving speed

Figure 19 Spectra of the decomposed components under different test conditions

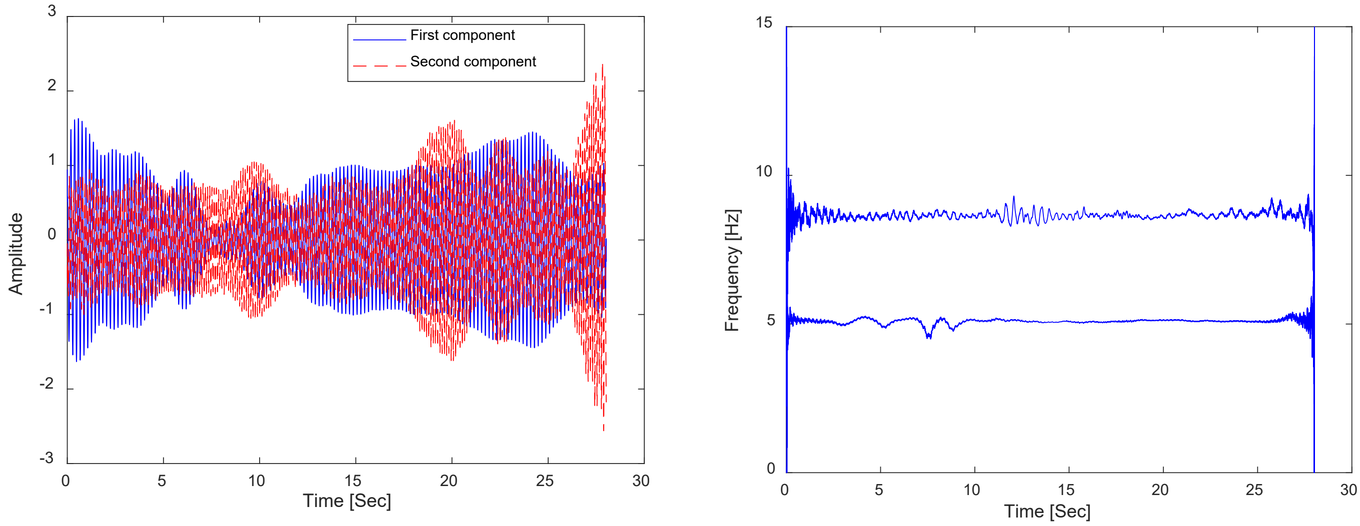

(a) The first two response components (b) The instantaneous frequencies

Figure 20 Response components and instantaneous frequencies